frontiers | Frontiers in Physics

TYPE Brief Research Report
PUBLISHED 13 June 2025
DOI 10.3389/fphy.2025.1623258

Check for updates

OPEN ACCESS

EDITED BY
Zhiyong Liu,
Southeast University, China

REVIEWED BY
Guojian Liu,
Suzhou University of Science and Technology, China
Yunjian Li,
Macau University of Science and Technology, Macao SAR, China

*CORRESPONDENCE
Jinyang Jiang,
jiangjinyang16@163.com

†These authors have contributed equally to this work and share first authorship

RECEIVED 05 May 2025
ACCEPTED 03 June 2025
PUBLISHED 13 June 2025

CITATION
Yang S, Zhang J, Zhang W, Dong Q, Xiang L, Sun G and Jiang J (2025) Study on the evolution mechanism of concrete properties under the coupled effects of freeze-thaw cycle, chloride salt and fatigue loading. *Front. Phys.* 13:1623258.
doi: 10.3389/fphy.2025.1623258

Study on the evolution mechanism of concrete properties under the coupled effects of freeze-thaw cycle, chloride salt and fatigue loading

Siqi Yang[1†], Jiawen Zhang[1,2†], Weijie Zhang[1], Qi Dong[1], Li Xiang[3], Guoxing Sun[4] and Jinyang Jiang[1,2]*

[1]School of Materials Science and Engineering, Southeast University, Nanjing, China, [2]State Key Laboratory of Engineering Materials for Major Infrastructure, Southeast University, Nanjing, China, [3]Jiangsu Key Laboratory for Design and Manufacturing of Precision Medical Equipment, School of Mechanical Engineering, Southeast University, Nanjing, China, [4]Joint Key Laboratory of the Ministry of Education, Institute of Applied Physics and Materials Engineering, University of Macau, Taipa, Macao SAR, China

The long-term durability performance of ballastless track systems exhibits significant dependence on their in-service environmental conditions. In addition to cyclic fatigue loading from train operations, critical durability challenges arise from the coupled effects of freeze-thaw cycling and chloride ion penetration, particularly in coastal regions or cold climate zones. Conventional experimental studies predominantly focus on single or dual-factor acceleration tests and confined to macroscopic performance characterization. In this study, the coupling effect of freeze-thaw, chloride salt and loading on the microstructure evolution was systematically and quantitively investigated, with the role of each kind of environmental action analyzed, experimentally and quantitively evaluating the significantly greater damage by freeze-thaw and chloride salt erosion to concrete than that of fatigue load.

KEYWORDS

ballastless track, freeze-thaw cycles, chloride salt, fatigue load, microstructure

1 Introduction

Ballastless tracks are preferred in high-speed rail systems for their minimized maintenance requirements and durability [1]. Concrete serves as the primary material for their construction [2], which must endure repeated train loads and harsh environmental conditions [3], including subzero temperatures [4] and saline soils that accelerate degradation [5, 6]. In permafrost regions, subzero winter temperatures induce critical durability challenges such as surface scaling, internal freeze-thaw-induced expansion cracking, and strength reduction in track concrete. Ballastless tracks in saline soil environments face accelerated degradation from combined freeze-thaw conditions and chloride salt erosion. During practical service, concrete suffers combined damage from load and environmental stress, necessitating research into how fatigue and environmental factors affect its performance over time [7].

To date, the deterioration mechanisms of concrete under the freeze-thaw single factor condition have been systematically investigated. Xiong et al. [8] found that the extent of freeze-thaw damage in concrete was intrinsically linked to the physicochemical characteristics of hydration products and pore structure. The impact of load under the combined effects of freeze-thaw and chloride have also been examined. Extending to the coupled conditions of freeze-thaw cycles and chloride attack, some scholars have analyzed the internal and external factors affecting the degree of concrete damage [9]. Internal factors primarily encompass pre-existing microcracks, hydration phase compositions, and pore network architecture, while external variables are quantified through freeze-thaw cycles and chloride concentration [10]. Guo et al. [4] found the coupled effect of freeze-thaw cycles and chloride attack causes more severe concrete deterioration than freeze-thaw action alone. Furthermore, the damage and deterioration mechanisms of concrete under coupled freeze-thaw cycles and fatigue loads were investigated [11]. Liu [12] and Zhang et al. [13] revealed the damage of prestressed concrete was initially caused by freeze-thaw cycles and then by fatigue with a life prediction model developed [14]. Macroscopically, concrete permeability and chloride ion transport behavior based on pore structure under the coupling action of load and chloride salt was surveyed [15–17], establishing quantitative relationships between pore structure characteristics and ionic diffusion/water transport. However, current research on this topic mainly just focuses on the coupled effect of two factors, limiting the precision of durability prediction. Research on the coupling effect of the freeze-thaw cycle, chloride erosion, and fatigue load is still lacking, so are the understanding of microstructural mechanism behind [18]. The common methods for evaluating the freeze-thaw durability of concrete are the mass loss rate and the modulus of the relative dynamic model [19]. These commonly used evaluation indicators have very limited reflections on the damage and durability of concrete. In addition, under the coupled effect of multiple factors, the durability of concrete will exhibit a more complex degradation mechanism than the effect of a single factor. It is difficult to correctly explain the mechanism of the decline in the durability of concrete only from the changes in mass and dynamic elastic modulus [20]. Therefore, in order to evaluate the durability performance of concrete more scientifically and comprehensively, it is necessary to combine microscopic testing techniques to characterize key indicators such as hydration products, pore structure and crack morphology inside the concrete [21]. Experimental studies on the durability and microscopic mechanism of concrete under the coupling action of multi-stage repeated freeze-thaw and chlorides are relatively lacking, and the damage mechanism of concrete under the coupling action of freeze-thaw, chlorides and fatigue has not yet formed a system. To better understand the performance evolution and damage state of concrete under real environment, such knowledge gap was filled in this study. The coupling study of freeze-thaw, chloride salt and fatigue load were divided into three stages: freeze-thaw and chloride salt erosion, fatigue load and subsequent freeze-thaw and chloride salt erosion, and the evolution of mechanical properties and durability of concrete was studied in each stage. Complementary microstructure characterization techniques, e.g., X-ray diffraction (XRD), scanning electron microscopy (SEM), and mercury intrusion porosimeter (MIP) are used to detect composition changes, morphological changes, and pore structure changes. This study comprehensively combines macro and microscale observation, analyzing the damage mechanism of concrete by relating the micropore parameters to mechanical properties parameters. This study provides new insights for the damage mechanism, performance prediction and material optimization design of ballastless track concrete system under complex coupling actions.

2 Method

In this study, C60-grade concrete specimens measuring 100 mm × 100 mm × 400 mm were prepared (detailed preparation procedure and recipe shown in Supplementary Material, Supplementary Table S1). Following 28 days of standard curing, the specimens underwent coupled freeze-thaw cycling and chloride attack testing through immersion in sodium chloride solutions at mass concentrations of 0%, 5%, and 10%. The freeze-thaw cycling was conducted following GB/T 50082-2009. The highest temperature in the center of the test piece was 6°C, and the lowest was −17°C. Each freezing-thawing cycle involved 2.5 h of the freezing process and 1.4 h of the thawing process. Thus, each cycle took 3.9 h. [22]. Mass change and relative dynamic elastic modulus [23] were monitored at 25-cycle intervals using precision weighing and ultrasonic pulse velocity measurements, respectively. After each testing phase, specimens were systematically reoriented within their containers, and fresh solutions were replenished to maintain consistent exposure conditions until the target number of cycles was achieved. Post-testing chloride profiling was performed on specimens exposed to 5% and 10% NaCl solutions, with chloride content analyzed at incremental depths [24] (0–5 mm, 5–10 mm, and 10–15 mm) following JTS/T 236-2009. The fatigue loading performances of the concrete was evaluated by performing four-point bending fatigue tests. The fatigue loading parameters were chosen based on the on-site service monitoring and experimental research of ballastless track concrete in the literature [23, 25]. The long-term cyclic and reciprocating train load was approximately regarded as sinusoidal fatigue loading with constant amplitude. The maximum stress level of fatigue loads was selected as 0.6, the action frequency was 20 Hz with a stress ratio of 0.5. Non-destructive evaluation of relative dynamic modulus was systematically performed at 5×10^4-cycle intervals using resonant frequency measurements.

In this experiment, two parallel control tests were established. The first group (FT-C-F1) underwent 50 freeze-thaw cycles with chloride attack tests, followed by 10^5 fatigue load cycles, and concluded with another 50 freeze-thaw cycles and chloride coupling tests. The second group (FT-C-F2) was subjected to 100 freeze-thaw cycles and chloride coupling tests, then 5×10^4 fatigue load cycles, and finally another 50 freeze-thaw cycles and chloride coupling tests. Multi-phase microstructural characterization was implemented using XRD, SEM, and MIP at four critical states [1]: initial state [2], post coupled effects freeze-thaw cycling and chloride attack [3], post-fatigue loading, and [4] post-coupled deterioration.

3 Results

3.1 Mechanical properties and durability of concrete

3.1.1 Effect of coupling action on the mass of concrete

Before the freeze-thaw test begins, the concrete samples with a curing age of 28 days are immersed in pure water for 4 days to reach saturation under room temperature based on GB/T 50082-2009 [26]. The rate of mass change refers to the ratio of the difference between the test mass and the mass of the concrete after soaking to the mass of the concrete after soaking. Figure 1a illustrates the mass changes of concrete specimens in group FT-C-F1 immersed in pure water, 5% and 10% sodium chloride solution during the first and third stage. After the first 50 freeze-thaw cycles, the mass of all specimens increased slightly. This should be because that after freeze-thaw treatment, additional pores and micro-cracks have formed inside the concrete [27], promoting the transfer of water to the deeper layers of the concrete, thereby increasing the mass of the concrete. During the fatigue loading stage, the free water in the concrete continuously dries and evaporates. The quality of concrete in each group decreased significantly, among which the mass of concrete in the 5% sodium chloride solution decreased the most [28]. After the last 50 freeze-thaw cycles, the defects in the concrete in the 5% sodium chloride solution were the greatest, and the degree of surface spalling was the highest. Therefore, its mass loss rate was also the highest. This indicates that throughout the entire experiment, the concrete in the 5% sodium chloride solution suffered the most severe damage [29].

Figure 1b presents the mass changes of concrete specimens in group FT-C-F2. In the first stage, all specimens exhibited mass similar increases within the 50th freeze-thaw cycle, particularly, from the 75th cycle, only specimens in pure water continued to gain mass, while those in 5% and 10% sodium chloride solutions experiences mass loss, with the 5% solution causing more decrease. [28]. In the third stage, specimens in pure water had a significant mass reduction, whereas those in sodium chloride solutions displayed minimal changes [29].

Overall, the mass loss of concrete in FT-C-F2 is greater than that in FT-C-F1 due to higher cycles of freeze-thaw. Particularly, the fatigue in stage II resulted in evident deviation of the mass behavior of specimens in pure water during the afterwards freeze-thaw cycles. With the total 75th and 100th freeze-thaw cycles, with fatigue coupling, the damage of specimen in water evidently resulted in mass loss. Contrastingly, without the fatigue loss, the mass of specimen in water still increased, which started to drop after the fatigue coupling and total 125th freeze-thaw cycles. In addition, for group FT-C-F1, the mass loss of concrete in 5% sodium chloride solution is the largest, while that in pure water is the largest for group FT-C-F2.

3.1.2 Effect of coupling action on dynamic elastic modulus of concrete

Figure 1c illustrates the variations in dynamic elastic modulus for the FT-C-F1 group. In the initial stage, all samples experienced a slight decrease in modulus, with the largest reduction in pure water (4.97%), followed by 5% sodium chloride (3.87%), and the smallest in 10% sodium chloride (2.10%). In the second stage, the modulus constantly decreased in a trend 10% sodium chloride solution (0.25%) < pure water (3.23%) < and 5% sodium chloride (4.68%). Such results suggested that the damage already occurred during the first 50th freeze-thaw for specimens, especially that in 5% chloride solution, which could not be differentiated by mass measurement due to the simultaneous water absorption. In the third stage, the modulus dropped significantly for pure water (29.62%) and 5% sodium chloride (37.15%) due to cumulative damage, whereas 10% sodium chloride had a smaller reduction (8.70%), which were consistent with mass change results, suggesting that a higher mass loss should arise from more severe internal damage.

Figure 1d illustrates the dynamic elastic modulus variations of FT-C-F2 group, of which the trend is similar to the mass change results except that the mass increased while the modulus decreased during the first stage [30]. Such phenomenon further confirmed that during the freeze-thaw, the damage and water absorption occurred concomitantly, a higher mass gain did not suggest fewer damage, but the higher absorbed amount of water may induce more damage during freezing. As such, the specimen absorbed highest amount of water, i.e., specimen in water, were of lowest modulus after the third stage. The rate of dynamic elastic modulus loss of concrete in group FT-C-F2 was notably higher than in group FT-C-F1, indicating that freeze-thaw cycles had a more pronounced effect on the dynamic elastic modulus of concrete compared to fatigue loading. The rate of decline in dynamic elastic modulus increased with the number of freeze-thaw cycles, especially when the number of freeze-thaw cycles exceeds 50, the decline rate of dynamic elastic modulus of concrete increases sharply.

3.1.3 Chloride ion content in concrete under coupling action

Chloride ion content in FT-C-F1 concrete specimens was measured at depths of 0–5 mm, 5–10 mm, and 10–15 mm following the first and third stages of exposure to 5% and 10% sodium chloride solutions. After the first stage, chloride levels were 0.253%, 0.099%, and 0.022% for 5% sodium chloride solution, and 0.385%, 0.184%, and 0.039% for 10% sodium chloride solution, respectively, as shown in Figure 1e. Following the third stage, these values increased to 0.359%, 0.136%, and 0.030% for 5% sodium chloride solution, and 0.591%, 0.292%, and 0.069% for 10% sodium chloride solution, as depicted in Figure 1f.

The results indicate that the chloride ion content in each depth interval of the concrete exposed to 10% sodium chloride solution is not simply double that of the concrete exposed to 5% sodium chloride solution. This discrepancy can be attributed to differences in cumulative damage and pore structure between the two groups under coupled conditions. The porosity and damage within the concrete influence the transport of chloride ions [31]. The chloride ion content generally decreases with increasing concrete depth, with a faster initial rate followed by a slower decrease.

3.2 Morphology and microscopic characterization of concrete

3.2.1 Morphology of concrete

The morphology and microstructure changes after each stage were further surveyed by using FT-C-F1 group as an example.

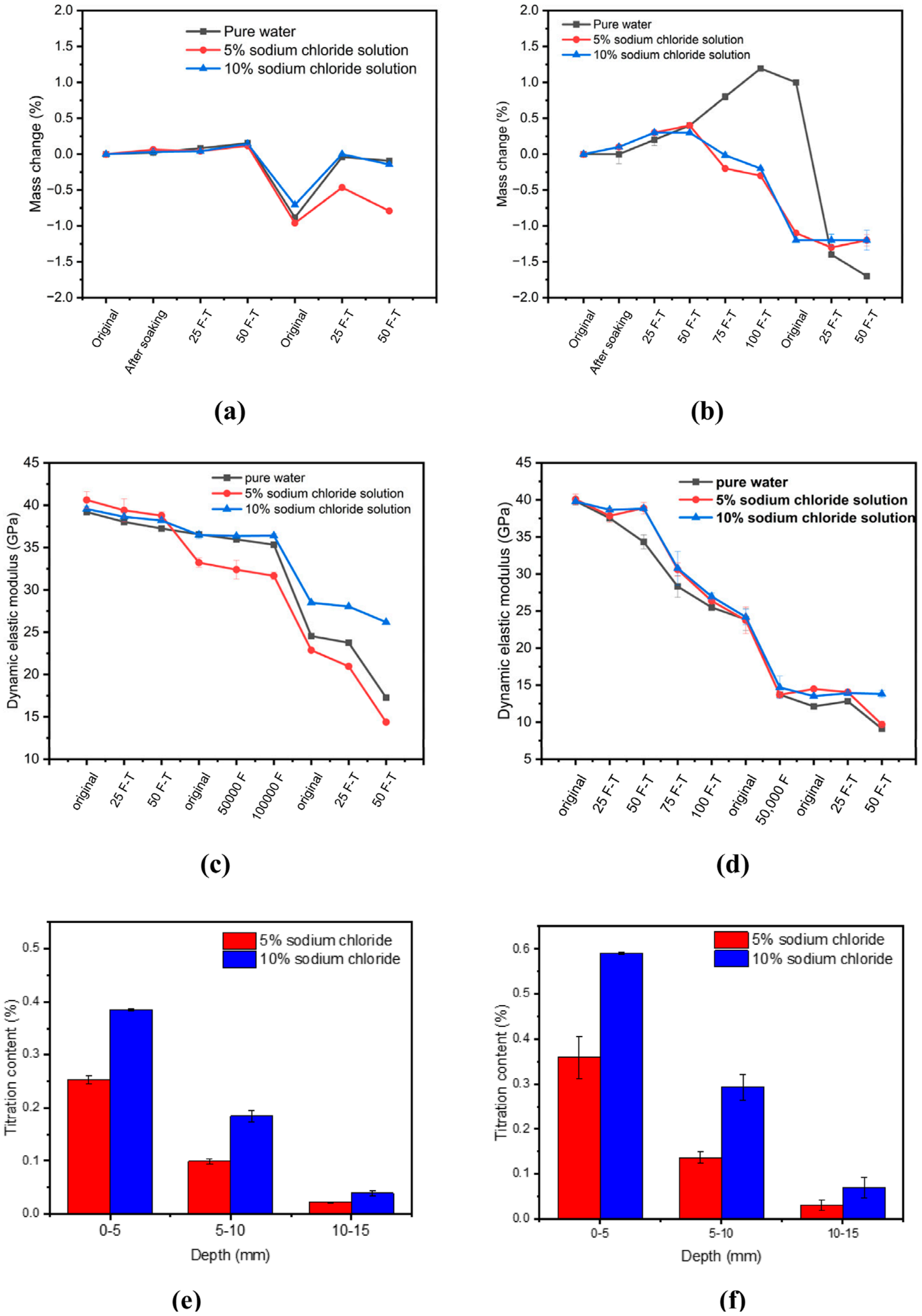

FIGURE 1
The rate of mass change in **(a)** FT-C-F1 and **(b)** FT-C-F2; Change trend of dynamic elastic modulus in **(c)** FT-C-F1 and **(d)** FT-C-F2; The relationship between chloride ion content and depth of concrete in the **(e)** first coupling tests and **(f)** subsequent coupling tests.

Following the first stage, visible pores emerged on the surface of the concrete in pure water (Figures 2a–c). The specimens exposed to a 5% sodium chloride solution exhibited the highest degree of damage, characterized by not only numerous pores but also slight spalling (Figures 2d–f). In contrast, while the 10% sodium chloride solution induced the formation of many pores on the surface, the overall structural integrity remained intact (Figures 2g–i). By the third stage, degradation intensified across all groups with trend:

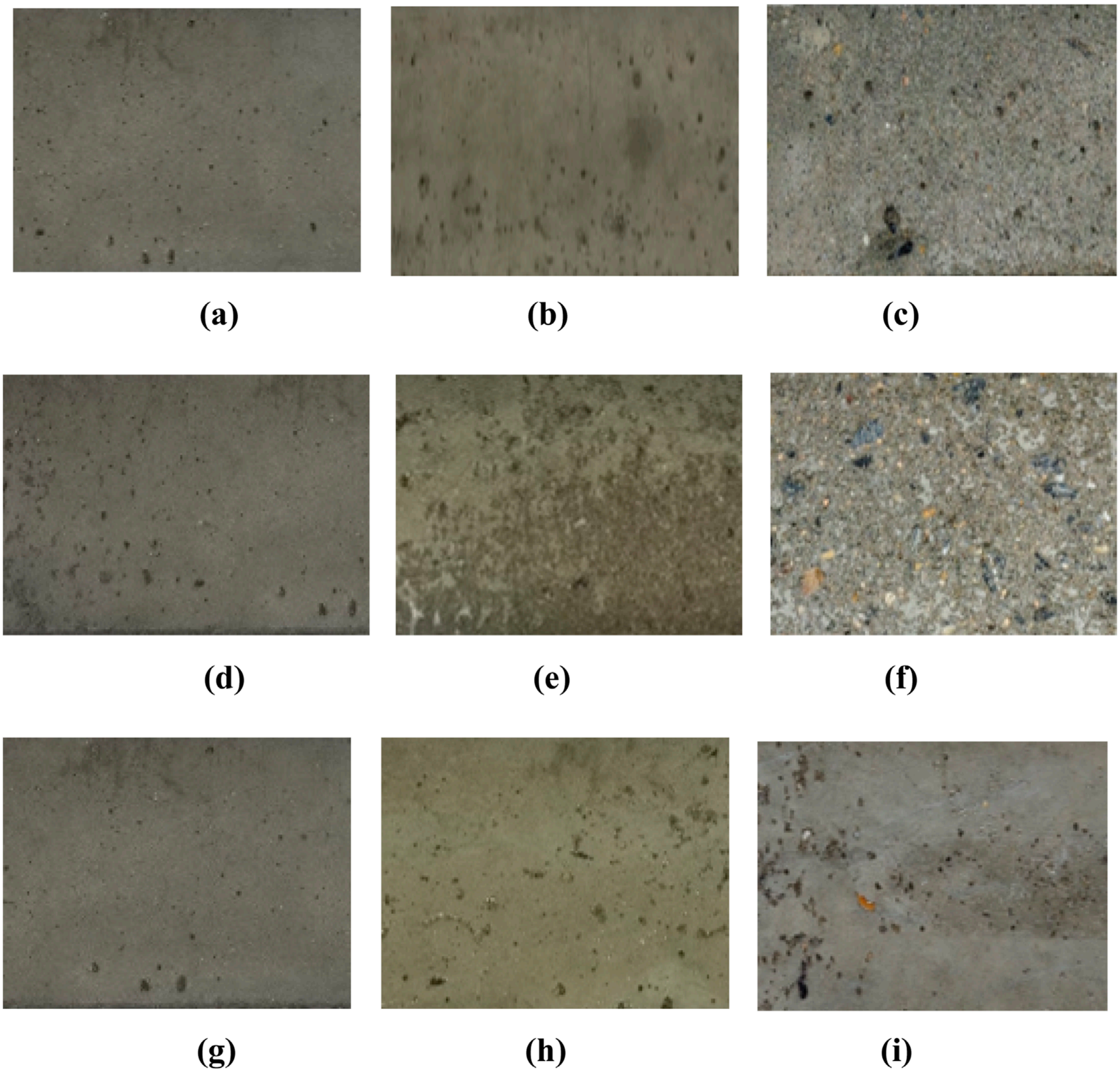

FIGURE 2
Concrete morphology under different conditions: **(a)** soaked in pure water, **(b)** after the first stage, **(c)** after third stage; **(d)** soaked in 5% sodium chloride, **(e)** after the first stage, **(f)** after the third stage; **(g)** soaked in 10% sodium chloride, **(h)** after the first stage, **(i)** after the third stage.

5% sodium chloride solution < pure water <10% sodium chloride solution. Specimens in the 5% sodium chloride solution experienced pronounced spalling with substantial aggregate exposure and the greatest mass loss. Specimens in pure water showed substantial spalling without evident exposure of aggregate, forming large pores on the surface. The 10% sodium chloride solute group suffer only minor and localized delamination, representing the least severe deterioration.

3.2.2 Composition analysis

Concrete typically comprises river sand, stone, and cementitious materials, of which the hydration product contents and types in concrete under different corrosive environments may be distinct. To investigate the effect of water chemistry on the concrete composition, samples are taken from concrete at three different locations which are treated in pure water, 5% and 10% sodium chloride solutions after the first and third stages, respectively. In pure water (Figure 3a), initial C_2S (dicalcium silicate) and C_3S (tricalcium silicate) phases progressively convert to C-S-H (calcium silicate hydrate), while reactive Al_2O_3 from fly ash facilitates the transformation of alkaline C-H (calcium hydroxide) into C-A-H (calcium aluminate hydrate) or C-A-S-H (calcium aluminate silicate hydrate), with its primary diffraction peak at 21.76° exhibiting decreasing intensity from surface to core, consistent with water transport dynamics. Under 5% sodium chloride immersion, SiO_2 and C-A-S-H dominate, whose peaks are at 21.76° and 37.42°, featuring trace ettringite (AFt) and residual $CaSiO_3$, reflecting incomplete hydration, as shown in Figure 3b). In a 10% sodium

10.3389/fphy.2025.1623258

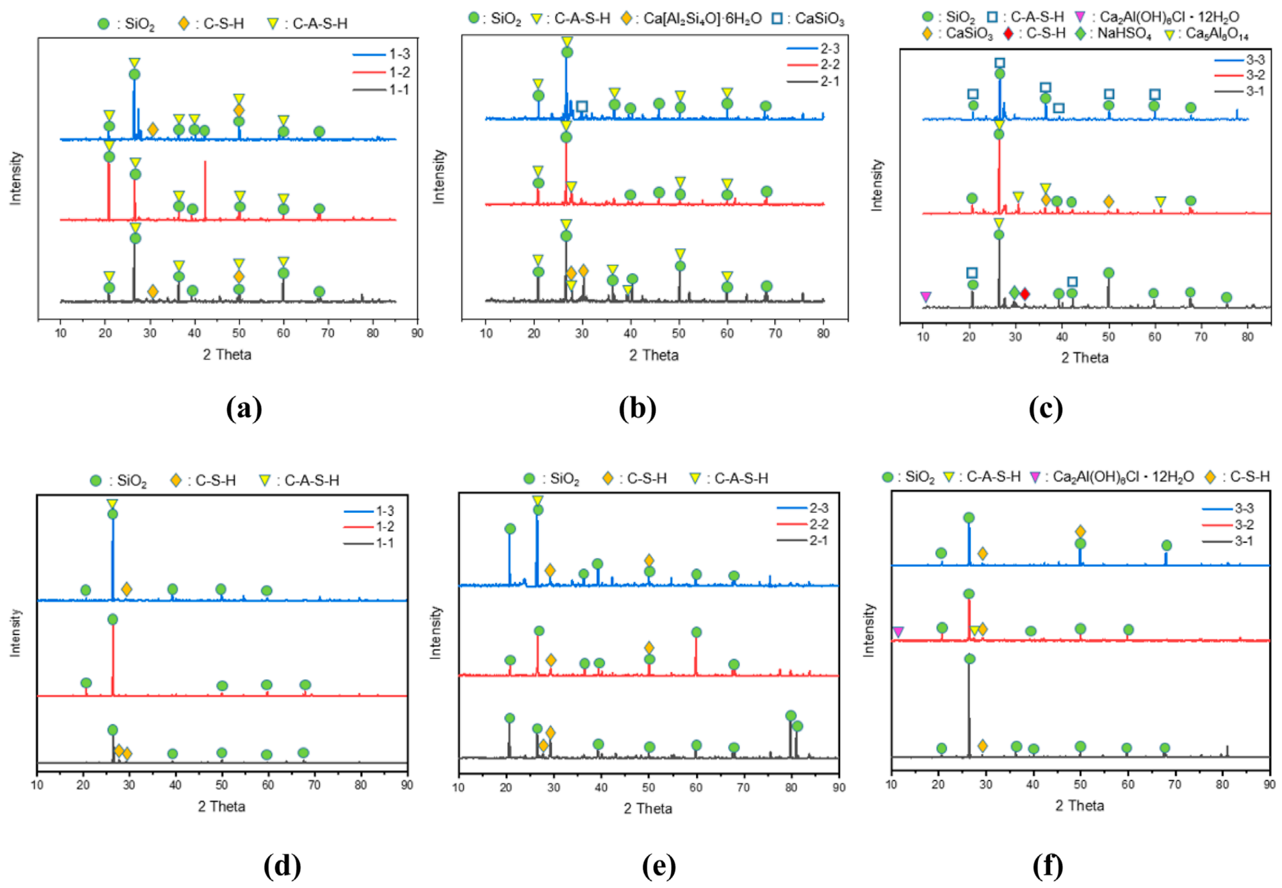

FIGURE 3
XRD pattern of concrete after the first stage in **(a)** pure water, **(b)** 5% sodium chloride, and **(c)** 10% sodium chloride; after the third stage in **(d)** pure water, **(e)** 5% sodium chloride, and **(f)** 10% sodium chloride.

chloride solution, the main components of concrete are also SiO_2 and C-A-S-H. As depicted in Figure 3c, small amounts of C-S-H and Friedel's salt are present within 0–5 mm. Due to the large pores in the interfacial transition zone, chloride ions react with calcium aluminate hydrate ($CaO{\cdot}Al_2O_3{\cdot}10H_2O$) at the interface to form Friedel's salt. This compound continues to react with the hydration product C-H crystals to form water-soluble $CaCl_2$ and small amounts of $CaSiO_3$ are also detected.

After the third stage, the main components of each group of samples are SiO_2, C-A-S-H, and C-S-H, as shown in Figures 3d–f. Compared to the first stage, the contents of C-A-S-H and C-S-H at each depth significantly decreased, while the diffraction peak intensity of hydration products increased with depth. Such phenomenon suggests that the exposure of concrete in aqueous media results in Ca^{2+} and Al^{3+} leaching [32]. A small amount of Friedel's salt was detected in the concrete exposed to a 10% sodium chloride solution within 0–5 mm, which demonstrated that the formation of Friedel's salt was slow and occurred under high chloride concentration.

3.2.3 Micromorphology

To analyze the damage and deterioration mechanism of concrete more intuitively, SEM tests were conducted on concrete samples after the first and third stage. Even for concrete in the 10% sodium chloride solution, only trace amounts of Friedel's salt were detected after the third stage [33], thus the reaction effect on the chloride was not further discussed and the detailed results are shown in the Supplementary Material, Supplementary Figures S1, S2.

MIPS was utilized to examine the pore size distribution characteristics and evolution patterns of concrete [34]. Pore structure analysis of FT-C-F1 group concrete across three exposure stages revealed distinct evolutionary patterns (Figures 4a–i). The pore size distribution of concrete can be categorized into four types: gel pores (<10 nm), small capillary pores (10–100 nm), large capillary pores (100–1,000 nm), and macropores (>1,000 nm), which are closely related to the concrete performance [35]. The initial porosity for all the samples before treatments were similar. After the first stage, the porosity for all samples significantly increased with the extent follow the trend: 5% NaCl > pure water>10% NaCl. Such observation suggested that the freeze-thaw cycles profoundly affected the pore structures and porosity, which should be due to the internal stress induced by the ice crystal expansion [36]. After the second stage, the porosity did not change evidently, while some of them even decreased, indicating the pores might be compacted by the fatigue actions [37]. After the third step, the porosity further dramatically elevated, confirming the

10.3389/fphy.2025.1623258

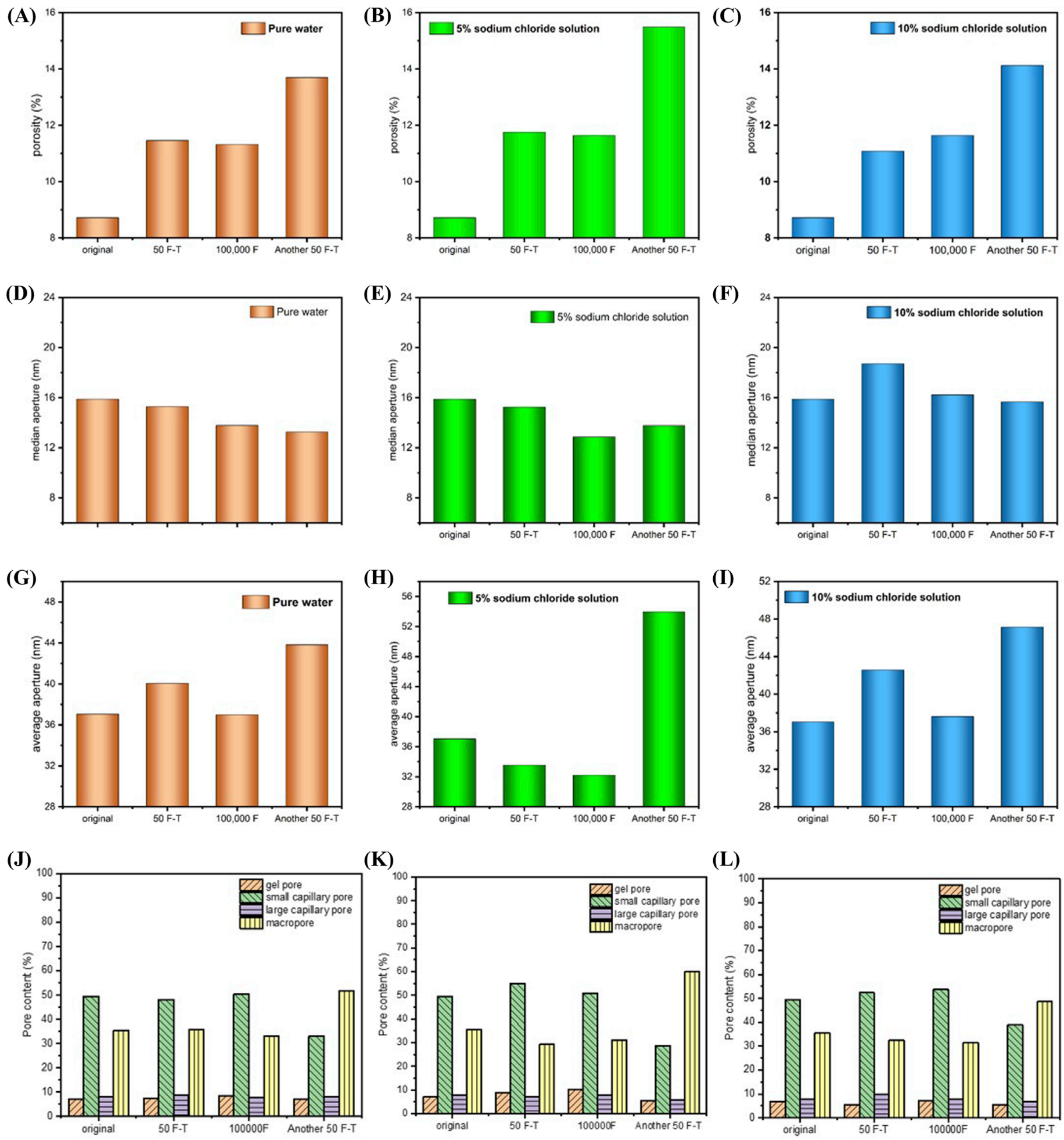

FIGURE 4
Concrete properties under different conditions: porosity in **(a)** pure water, **(b)** 5% sodium chloride, and **(c)** 10% sodium chloride; median aperture in **(d)** pure water, **(e)** 5% sodium chloride, and **(f)** 10% sodium chloride; average aperture in **(g)** pure water, **(h)** 5% sodium chloride and **(i)** 10% sodium chloride. Pore distribution of **(j)** pure water, **(k)** 5% sodium chloride solution and **(l)** 10% sodium chloride solution.

severe damage caused by freeze-thaw actions. The 5% sodium chloride solution environment exhibited a pronounced increase in both pore size and number, indicating severe deterioration, whereas pore development in 10% sodium chloride solution surpassed that in pure water, highlighting accelerated degradation. Such observation is consistent with the mass and modulus change results.

As to the median pore diameter, after first step, it decreased by 3.78% and 4.03% in pure water and 5% sodium chloride solution respectively, but increased 17.76% in 10% sodium chloride solution. After the second step, median pore sizes in pure water, 5% sodium chloride solution and 10% sodium chloride solution decreased by 9.82%, 15.62% and 13.26%, respectively. After the third stage, median pore sizes showed divergence, decreasing by 3.85% in pure water and 3.39% in 10% sodium chloride solution, but increasing by 7.08% in 5% sodium chloride solution. Therefore, there are no explicit trends for median pore diameter for each sample, which are possibly due to the numbers of pores with different sizes are all increased during the damage. During the environmental actions, gel pores or small capillary pores in concrete gradually expanded and evolved into larger capillary pores or macropores, while new pores continued to grow as gel pores and the number could be high. Therefore, comprehensively the median aperture that was statistically calculated based on counts may randomly change and did not show evident trend.

For the average pore diameter, after the first step, it showed 8.13% and 14.93% growth in pure water and 10% sodium chloride solution groups, contrasting with a 9.45% reduction in 5% sodium chloride solution, which, after the second step, declined by 7.67%, 4.00%, and 11.65%, respectively. After the third stage, average pore size of concrete in pure water, 5% sodium chloride solution and 10% sodium chloride solution increased by 18.47%, 67.52% and 25.31%. The evolution trending of average aperture was observed to similar to that of porosity, while distinctive with median aperture. This should be attributed to that the porosity and average aperture are both significantly affected by the pore volume, and for the macro size pore. The number increase of macropores would affect the average aperture much more than that of gel pores, which are attributed to that its size increase extent should be much higher than that of gel pores.

As illustrated in Figures 4j–l, approximately 50% of the total pore volume is composed of small capillary pores, while macropores constitute around 30%. Gel pores and large capillary pores each account for less than 10% of the total pore volume. After the first and second stage, the content of gel pores and small capillary pores are basically increased while the content of large capillary pores and macropores, suggesting that at these stages, the production of new pores surpass the growth of pore size. Such phenomenon could be used to explain the median aperture for samples in pure water and 5% sodium chloride solution decreased in these stages. As to the third stage, the content of gel pores and especially small capillary pores decreased, while the content of macropores dramatically increased [38]. Such observation demonstrated that at the third stage, the inner structures of concrete were severely damaged, and the extent of the transition of small pores to macropores significantly exceeded the growth of small pores. And the macropores trending are consistent with the modulus change trending, explaining the macroscopic mechanical property revolution from the quantitively microstructure evolution. As to the large capillary pores, their number did not change evidently, indicating that once the small pores expanded, they would mostly evolve into macropores. It should be noted that, under fatigue loading, though the proportion of large capillary pores or macropores decreased due to compactness, gel pores and small capillary pores still grew, which may cause more severe damage in the third stage when the freeze-thaw action was applied. Therefore, in the practical applications, when the fatigue loading and freeze-thaw action in presence of chloride ions are simultaneously applied on concretes, the concretes would show more severe damage compared with the concrete under freeze-thaw action with chloride ions.

4 Discussion

This study implemented three-stage coupling procedures for investigating concrete under controlled exposure conditions. The critical performance indicators including mass variation, dynamic elastic modulus, and chloride ion content were systematically monitored, the degradation of mechanical properties and durability was also surveyed. In the first stage, for concrete in pure water, the maximum mass increase rate was <0.2% with 50 freeze-thaw cycles and remained consistent until 100 cycles. In the third stage, the increase rate reached up to 1.2%. For concrete in chloride solution, after more than 50 freeze-thaw cycles, the mass loss rate for concrete in a 5% chloride solution reached 1%. In the third stage, both FT-C-F1 and FT-C-F2 showed significant mass loss rates in the 5% chloride solution, at 0.8% and 1.2%, respectively. The impact of freeze-thaw cycles on concrete mass is notably greater than that of fatigue loading.

As to the dynamic elastic modulus, for FT-C-F1 after the first stage in pure water, it decreased by up to 4.97%. However, the dynamic elastic modulus of concrete in a 5% sodium chloride solution after the first stage decreased more significantly compared to that in pure water, resulting in a final loss of 64.61%. For FT-C-F2, the decrease in dynamic elastic modulus in pure water during the first stage was the most substantial, at 36.02%. In the third stage, the rate of decrease in dynamic elastic modulus for concrete in a 5% chloride solution was faster than that in pure water. However, the dynamic elastic modulus decreased by 10.4% and 12.3% for concrete in pure water and 5% sodium chloride solution respectively after the second stage, which means a more limited additional degradation even after numerous cycles. Overall, the effect of freeze-thaw cycles on the dynamic elastic modulus of concrete is more pronounced than that of fatigue loading. However, the fatigue loading was revealed to initiate the production of small pores, resulting in the dramatical transition from small pores to macropores. Hence, the coupling of fatigue with freeze-thaw in presence of chloride ions deteriorate the concrete not by the fatigue load itself but through elevating the damage of freeze-thaw action.

Besides, freeze-thaw cycles promote the development of concrete pores, particularly impacting larger pores. Within a certain number of cycles, fatigue loading promotes a reduction in concrete porosity, which leads to 0.1386% and 0.1176% for pure water and 5% sodium chloride solution respectively, mainly affecting smaller pores. The increase in pore number and volume has a significant effect on the dynamic elastic modulus of concrete, while the transport of chloride ions is influenced by the number of detrimental pores.

In this study, the coupling effects of fatigue with freeze-thaw in saline solution were systematically studied, and it was revealed that the mechanical properties distinctively deviated from coupling effect of two environmental factors. Further, the correlation between the microstructure of concrete pores and its mechanical properties was investigated, which provided microscale insights into the evolution of macroscopic mechanical properties and the unveiled damage mechanisms can facilitate better prediction the performance of ballastless track.

Data availability statement

The raw data supporting the conclusions of this article will be made available by the authors, without undue reservation.

Author contributions

SY: Formal Analysis, Conceptualization, Writing – original draft, Methodology. JZ: Formal Analysis, Writing – review and editing. WZ: Data curation, Writing – original draft. QD: Writing – review and editing, Visualization, Resources. LX: Funding acquisition, Writing – review and editing, Formal Analysis. GS: Investigation, Resources, Writing – review and editing. JJ: Supervision, Writing – review and editing, Project administration.

Funding

The author(s) declare that financial support was received for the research and/or publication of this article. This work was supported by the International Cooperation and Exchange of the National Natural Science Foundation of China (52261160646), the National Natural Science Foundation of China (52379119, 52305185), the Science and Technology Development Fund, Macao SAR [File no.0076/2022/AFJ].

Conflict of interest

The authors declare that the research was conducted in the absence of any commercial or financial relationships that could be construed as a potential conflict of interest.

Generative AI statement

The author(s) declare that no Generative AI was used in the creation of this manuscript.

Publisher's note

Supplementary material

The Supplementary Material for this article can be found online at: https://www.frontiersin.org/articles/10.3389/fphy.2025.1623258/full#supplementary-material

References

1. Yan B, Tian JH, Huang J, Lou P. Fatigue characteristics of long-span bridge-double block ballastless track system. *Mathematics* (2023) 11(8):1792. doi:10.3390/math11081792

2. Zhang JW, Cai CBA, Zhu SY, Wang MZ, He QL, Yang SF, et al. Experimental investigation on dynamic performance evolution of double-block ballastless track under high-cycle train loads. *Eng Structures* (2022) 254:113872. doi:10.1016/j.engstruct.2022.113872

3. Sun W, Mu R, Lua X, Miao CW. Effect of chloride salt, freeze-thaw cycling and externally applied load on the performance of the concrete. *Cement Concrete Res* (2002) 32(12):1859–64.

4. Guo K, Tong Z, Zhang S, Pan W, Liu L. Durability of GO-RAC under the coupling action of freeze-thaw cycling and chloride salt erosion. *J Building Mater* (2023) 26(11):1183–91.

5. Yang Q. One of mechanisms on the deicer-frost scaling of concrete(?):degree of saturation and ice-formation pressure during freezing-thawing cycles. *J Building Mater* (2012) 15(6):741–6.

6. Yang L, Pang Y, Tang Q, Chen X, Gao D, Li H, et al. Effects of the stearic acid modified mica powder on hydrophobic properties and salt freezing resistance of mortar: experimental study and microscopic mechanism analysis. *Construction Building Mater* (2024) 416:135188. doi:10.1016/j.conbuildmat.2024.135188

7. Cao Y, Wang L, Wang Z, Yao Y. Deterioration of concrete caused by freeze-thaw cycles combined with chloride attack under flexural load. *J Building Mater* (2016) 19(5):821–5.

8. Xiong B, Gao L, Lu X, Tian B, Chen B. Freezing-thawing failure evolution model of concrete based on hydrostatic pressure theory. *Eng Mech* (2023) 40(4):184–92.

9. Li H, Guo HL, Zhang Y. Deterioration of concrete under the coupling action of freeze-thaw cycles and salt solution erosion. *Rev Advanced Mater Science.* (2022) 61(1):322–33. doi:10.1515/rams-2022-0025

10. Guo JJ, Sun WQ, Xu YQ, Lin WQ, Jing WD. Damage mechanism and modeling of concrete in freeze-thaw cycles: a review. *Buildings* (2022) 12(9):1317. doi:10.3390/buildings12091317

11. Qiao YF, Sun W, Jiang JY. Damage process of concrete subjected to coupling fatigue load and freeze/thaw cycles. *Construction Building Mater* (2015) 93:806–11. doi:10.1016/j.conbuildmat.2015.05.087

12. Liu R, Zhang Y, Chen Y, Liu T. Fatigue damage model of prestressed concrete beams suffered freeze-thawing. *J Jiangsu University* (2012) 33(1):115–9.

13. Zhang Y, Hu Q, Chen Y, Liu R. Bending performance test and numerical simulation of prestressed concrete beams after freeze-thaw. *Industrial Construction* (2015) 45(2):27–31.

14. Hong J, Miao C, Huang W, Liu J, Wan Y. Influence of freeze-thaw damage on the fatigue life of concrete. *China Civil Eng J* (2012) 45(6):83–9.

15. Ecay L, Grégoire D, Pijaudier-Cabot G. On the prediction of permeability and relative permeability from pore size distributions. *Cement Concrete Res* (2020) 133:106074. doi:10.1016/j.cemconres.2020.106074

16. Khaddour F, Grégoire D, Pijaudier-Cabot G. A hierarchical model for the computation of permeation properties of porous materials and their enhancement due to microcracks. *J Eng Mech* (2018) 144(2). doi:10.1061/(asce)em.1943-7889.0001392

17. Li Y, Shen A, Lyu Z, Guo Y. Investigations of chloride ions permeability of pavement concrete under coupled effect of fatigue loading and hydrodynamic pressure. *International J Pavement Eng* (2022) 23(5):1659–74. doi:10.1080/10298436.2020.1819540

18. Chen C, Zhang K, Ye L. Influence of freeze-thaw cycles and sustained load on the durability and bearing capacity of reinforced concrete columns. *Materials.* (2024) 17(24):6129. doi:10.3390/ma17246129

19. Kong Z, Lu N. Improved method to determine young's modulus for concrete cylinder using electromechanical spectrum: principle and validation. *J Aerospace Eng* (2020) 33(6). doi:10.1061/(asce)as.1943-5525.0001196

20. Xiao J, Lv Z, Duan Z, Zhang C. Pore structure characteristics, modulation and its effect on concrete properties: a review. *Construction Building Mater* (2023) 397:132430. doi:10.1016/j.conbuildmat.2023.132430

21. Zhang D, Wang W, Li VC. Microcrack characterization of loaded Engineered Cementitious Composites via optical scans and photogrammetric analyses. *Construction Building Mater* (2022) 318:126000. doi:10.1016/j.conbuildmat.2021.126000

22. He R, Nantung T, Lu N. Unraveling microstructural evolution in air-entrained mortar and paste: insights from MIP and micro-CT tomography amid cyclic freezing-thawing damage. *J Building Eng* (2024) 94:109922. doi:10.1016/j.jobe.2024.109922

23. Ren JJ, Deng SJ, Wei K, Li HL, Wang J. Mechanical property deterioration of the prefabricated concrete slab in mixed passenger and freight railway tracks. *Construction Building Mater* (2019) 208:622–37. doi:10.1016/j.conbuildmat.2019.03.039

24. Gao D, Yang L, Pang Y, Li Z, Tang Q. Effects of a novel hydrophobic admixture on the sulfate attack resistance of the mortar in the wet-dry cycling environment. *Construction Building Mater* (2022) 344:128148. doi:10.1016/j.conbuildmat.2022.128148

25. Ren J, Du W, Deng S, Feng X. Chloride ion transport in concrete of ballastless track under fatigue loading. *J Southwest Jiaotong University* (2021) 56(3):510–6.

26. He R, Lu N. Hydration, fresh, mechanical, and freeze-thaw properties of cement mortar incorporated with polymeric microspheres. *Advanced Composites Hybrid Mater* (2024) 7(3):92. doi:10.1007/s42114-024-00899-2

27. Sellevold EJ, Farstad T. *Frost/salt-testing of concrete: effect of test parameters and concrete moisture history. Nordic concrete research* (1991). p. 121–38.

28. Li F, Fan S, Xiao S, Huo J, Yuan Y, Chen Z. Flexural performance and damage of reinforced fly ash and slag-based geopolymer concrete after coupling effect of freeze-thaw cycles and sustained loading. *Structures* (2024) 64:106537. doi:10.1016/j.istruc.2024.106537

29. Feng B, Liu Q, Qian Y. Durability analysis of high-performance concrete under chloride salt erosion and freeze-thaw cycles. *J Southwest Jiaotong University* (2023) 58(5):1083–9.

30. Chai L, Yue Z, Chen Z, Fan G, Wang L. Volume stability and frost resistance of high-ductility magnesium phosphate cementitious concrete. *Materials.* (2024) 17(11):2522. doi:10.3390/ma17112522

31. Li F, Fan S, Cai C, Huo J, Su Q, Jin H, et al. Comprehensive research of the durability, bending deterioration and micro properties of lining concrete in an environment with bending stress-chloride salt-large temperature difference coupling. *Construction Building Mater* (2024) 439:137337. doi:10.1016/j.conbuildmat.2024.137337

32. Chai L, Yue Z, Guo L, Huang Y, Chen B. Mechanical constitutive behavior and microstructure evolution of high ductility concrete rapid repair material at different curing ages. *Construction Building Mater* (2025) 458:139600. doi:10.1016/j.conbuildmat.2024.139600

33. Yun-qing Z, Hong-fa YU, Jia-chun W. Study of surface damage rule of concrete structure exposed to salt freezing condition. *China J Highway Transport* (2009) 22(4):57–63.

34. Gan L, Zou ZY, Zhang ZL, Zhang HW, Gu H, Jin HJ. Investigation on the evolution of concrete pore structure under freeze-thaw and fatigue loads. *J Building Eng* (2024) 97:110914. doi:10.1016/j.jobe.2024.110914

35. Elakneswaran Y, Nawa T, Kurumisawa K. Electrokinetic potential of hydrated cement in relation to adsorption of chlorides. *Cement Concrete Res* (2009) 39(4):340–4. doi:10.1016/j.cemconres.2009.01.006

36. Sánchez I, Novoa XR, de Vera G, Climent MA. Microstructural modifications in Portland cement concrete due to forced ionic migration tests. Study by impedance spectroscopy. *Cement Concrete Res* (2008) 38(7):1015–25.

37. Li ZN, Shen AQ, Long HJ, Guo YC, He TQ. Dynamic deterioration of strength, durability, and microstructure of pavement concrete under fatigue load. *Construction Building Mater* (2021) 306:124912. doi:10.1016/j.conbuildmat.2021.124912

38. Farnam Y, Washington T, Weiss J. The influence of calcium chloride salt solution on the transport properties of cementitious materials. *Advances in Civil Eng* (2015) 2015:1–13. doi:10.1155/2015/929864